PCCP

Accepted Manuscript

This is an *Accepted Manuscript*, which has been through the Royal Society of Chemistry peer review process and has been accepted for publication.

Accepted Manuscripts are published online shortly after acceptance, before technical editing, formatting and proof reading. Using this free service, authors can make their results available to the community, in citable form, before we publish the edited article. We will replace this *Accepted Manuscript* with the edited and formatted *Advance Article* as soon as it is available.

You can find more information about *Accepted Manuscripts* in the Information for Authors.

Please note that technical editing may introduce minor changes to the text and/or graphics, which may alter content. The journal's standard Terms & Conditions and the Ethical guidelines still apply. In no event shall the Royal Society of Chemistry be held responsible for any errors or omissions in this *Accepted Manuscript* or any consequences arising from the use of any information it contains.

ROYAL SOCIETY OF CHEMISTRY

www.rsc.org/pccp

Journal Name

ARTICLE

Surface-enhanced Raman scattering on silvered porous alumina templates: role of multipolar surface plasmon resonant modes

Received 00th January 20xx,
Accepted 00th January 20xx

DOI: 10.1039/x0xx00000x

www.rsc.org/

S. N. Terekhov,[a] S. M. Kachan,[b] A. Yu. Panarin,[a] P. Mojzes[c]

Nanostructured silver films with different thicknesses were prepared by the vapor deposition onto the surface of anodic aluminum oxide (AAO) template to be used as surface-enhanced Raman scattering (SERS) active substrates. Both peak position of surface plasmon resonance (SPR) band and SERS enhancement of silvered AAO samples displayed non-monotonous dependence on Ag layer thickness. Using 441.6 nm excitation and a water-soluble cationic Cu(II)-tetrakis(4-N-methylpyridyl) porphyrin (CuTMPyP4) as a SERS-reporting analyte, two maxima of the SERS enhancement were obtained for Ag layers of 15 and 120 nm thickness. Thickness dependencies have been analyzed taking into account type of SPR modes identified by means of quasicrystalline approximation (QCA) of statistical theory of multiple scattering of waves and multi-Lorentzian deconvolution. The analysis revealed that SERS enhancement is related to the absolute magnitude of distance between excitation wavelength and spectral position of collective SPR mode. It was shown that matching of excitation wavelength and the most intensive SPR modes with non-radiative decay, generated mainly by coherent interaction of higher-order plasmon resonant modes (quadrupole and octupole), play the dominate role in SERS performance. Besides, it has been observed that more intense SERS signal can be obtained when the analyte deposited on the Ag/AAO substrate was excited through the AAO template rather than from the silvered side. Our results demonstrate that appropriate excitation geometry and fine tuning of optical properties of Ag/AAO substrate by adjusting proper thickness of Ag layer with respect to particular excitation wavelength can contribute to more effective SERS enhancement.

1. Introduction

Surface-enhanced Raman scattering (SERS) spectroscopy is a label-free high-sensitive method for applications in analytical chemistry,[1,2] biomedicine,[3–6] sensor technology,[7,8] forensic science[9,10] and environmental monitoring.[11] The enormous enhancement of Raman signal occurs for molecules adsorbed on noble-metal surfaces with nanoscale roughnesses, so-called SERS-active substrates.[12,13] It is generally accepted that the SERS amplification is attributed by mainly two mechanisms: electromagnetic mechanism resulting from strong enhancement of local electromagnetic field near metallic nanostructures,[14,15] and chemical mechanism issuing from electronic resonance/charge transfer between adsorbed molecule and the metal surface.[16,17] The maximum contribution of the chemical enhancement to the SERS was evaluated to 10^2,[18] while enhancement via electromagnetic effect is evaluated to 10^8.[19] The dominant role of electromagnetic mechanisms in the Raman signal enhancement is due to the excitation of localized surface plasmon resonance (LSPR) which produces a huge local electromagnetic field, so-called "hot spots", close to metallic nanoparticles.

Optimization of the Raman amplification is of great interest for applying the SERS technique for analytical purposes and optical biosensing.[20,21] In this regard it is important to find the relationship between the LSPR position, the wavelength used for Raman excitation (λ_{ex}) and the SERS enhancement. There are two approaches to determine LSPR influence on SERS performance: the first one is to tune LSPR position at fixed excitation wavelength, the second one is to vary λ_{ex} for fixed LSPR features. It has been shown by several studies for metallic nanoparticles (NPs) of different shape that for a given excitation λ_{ex} the largest SERS intensity is reached when the LSPR position is located at the middle between the excitation λ_{ex} and the wavelengths of Raman scattering (λ_R).[22,23] However, it was also demonstrated that this rule not always applies. Relation between the SERS intensity and LSPR seems to depend also on some other factors, such as shape of nanoparticles[24-26] and excitation wavelength.[22,25,27] For example, in the case of NPs with elongated shape, like ellipsoids or nanowires, it was shown that SERS maximum is reached when the LSPR position is close to Raman wavelength λ_R.[24]

The Van Duyne's group was the first who studied the influence of the excitation wavelength on the SERS enhancement for triangular silver nanoparticles.[22] They have shown that regardless of λ_{ex}, the SERS intensity reaches maximum when

[a] B.I. Stepanov Institute of Physics NASB, Nezalezhnasti Ave., 68, 220072, Minsk, Belarus E-mail: terekhov@imaph.bas-net.by.
[b] Department of Information Technologies and Robotics, Belarusian National Technical University, Nezalezhnasti Ave. 65, 220013 Minsk, Belarus.
[c] Institute of Physics, Charles University in Prague, Ke Karlovu 5, CZ-121 16 Prague 2, Czech Republic.

This journal is © The Royal Society of Chemistry 20xx

Please do not adjust margins

Physical Chemistry Chemical Physics Accepted Manuscript

the LSPR is located within a spectral window of about 120 nm, width covering the excitation λ_{ex} and Raman λ_R wavelengths. That is, the SERS behaviour is governed by the rule: $\lambda_{ex}<\lambda_{LSPR}<\lambda_R$. A similar result was obtained for elongated NPs.[25] Several rules required to obtain the best SERS intensity depending on the nanoparticles shape at the fixed excitation wavelength were summarized in.[26]

Recently a fruitful approach to study correlation between plasmon resonance and SERS intensity by tuning plasmon resonance of deformable plasmonic nanostructures has been reported.[28-30] Hossain *et al.*[28] have demonstrated for gold nanoparticles deposited on an elastomeric membrane that mechanical plasmonic tuning could enable real-time control to optimize SERS sensitivity. Furthermore, it has been shown using a fix excitation line, that SERS signal of analytes deposited on stretchable nanoplasmonic structure consisted of silver particles sputtered on polydimethylsiloxane was increased when the excitation matched the plasmon resonance.[29] By using a deformable plasmonic membrane, a quantitative correlation between the plasmon resonance and the SERS signals was established: a particular SERS peak will reach its maximum at the maximum of products of the extinction values at an excitation wavelength and the corresponding Raman scattering wavelengths.[30]

The second approach to unveil LSPR – SERS-efficiency relation, i.e. variation of λ_{ex} at a fixed LSPR, was used in the study of silver triangular NPs excited by different wavelengths λ_{ex} from entire visible region.[31] It has been shown that the maximum SERS intensity is observed when the LSPR is located between the excitation and the Raman wavelengths. Similar results have been obtained for arrays of gold nanoellipses where the SERS enhancement was measured for three different laser lines.[23] All the above mentioned studies were performed for arrays of weakly coupled metal NPs, and showed a possibility to enhance SERS through optimization of nanoparticles size and shape.

However, significantly larger SERS enhancement can be obtained for arrays of closely packed metal nanoparticles, where strong near-field electromagnetic coupling between neighbouring particles leads to transformation of LSPR into collective surface plasmon resonance (SPR) band. In this case the enhancement of Raman signal is strongly affected by the gap between particles. It was shown that upon gradually reducing distance between coupled silver NPs of different shape and size (from 500 nm down to 70 nm), the SERS intensity increased up to two orders of magnitude in comparison with the non-coupled case.[32] This observation was confirmed also by Liu *et al*.[33]

Very few studies dealing with the influence of SPR features on the SERS performance for coupled nanoarrays were reported. Recently, the SPR-dependent investigation of the SERS enhancement was undertaken for silver nanoplates with three excitation wavelengths.[34] It has been found that Raman signals were greatly enhanced when the laser line matched the peak position of SPR band. Wang *et al*.[35] suggested that the criterion for maximum SERS enhancement in the case of silver nanocube-based two-dimensional substrates is a closeness between SPR and laser excitation wavelength λ_{ex}. Thus, the question on the relation between the SPR position and the SERS intensity for coupled nanoarrays still remains unresolved.

In the present paper, we report the study of 2D silver nanoarrays deposited at the surface of anodic aluminum oxide (AAO) as proper substrates for SERS with a special attention on the effect of SPR position on Raman enhancement. AAO characterized by a closely packed regular array of columnar pores, high reproducibility of preparation and modest cost fabrication becomes very popular material for producing various SERS-active structures. As examples of AAO-based SERS substrates can serve noble-metal nanowire arrays exhibiting strong SERS activity,[36,37] plasmon-resonant Au nanospheres and nanorods with different aspect ratios,[38] and Ag NPs deposited inside the pores.[39] Fabrication of three-dimensional (3D) nanostructures decorated with Au and Ag nanoparticles in AAO template, which provide high level of Raman enhancement, have also been demonstrated.[40,41] Recently, the AAO-based metal nanoarrays as SERS-active substrates have been further explored,[42-45] and the possibility of engineering highly effective nanostructures for SERS by evaporating silver in vacuum onto the surfaces of AAO substrate has been demonstrated.[46,47]

In this work, a series of silver-coated AAO templates (Ag/AAO) were prepared to study the influence of Ag mass thickness on the position of surface plasmon resonance, as well as the SERS performance. We have tuned the SPR features to yield the strongest SERS enhancement at a fixed excitation λ_{ex} by a gradual variation of the Ag film thickness. This approach allows to overcome limitations arising in the case of measurement spectra from a single substrate with many laser excitation wavelengths,[18,31] such as the needs to take into account various resonance conditions for analyte and to have a wide set of excitation sources.[22]

To assess SERS-activity of the AAO-based substrates, a water-soluble cationic Cu(II)-*tetrakis*(4-N-methylpyridyl) porphyrin (CuTMPyP4) was used as a probe molecule because of its well-assigned SERS spectrum and exceptional photostability. The analysis of experimental data was performed with the help of simulations based on the statistical theory of multiple scattering of waves. This allowed to identify contributions of different SPR modes, and to emphasize the role of higher-order plasmon resonance modes (quadrupole and octupole) with non-radiative decay in governing the SERS activity of the strongly coupled nanostructures like Ag/AAO.

2. Experimental Section

2.1 Chemicals and AAO films preparation

Cationic Cu(II)-*tetrakis*(4-N-methylpyridyl) porphyrin was synthesized according to standard procedures[48] by Dr. V.L. Malinovskii.

The AAO films were prepared in a two-step electrochemical anodization[49] with slight modifications. Aluminum foils with purity of 99.99% were used as a starting material. Before anodization process, foils were cleaned, degreased and

This journal is © The Royal Society of Chemistry 20xx

Physical Chemistry Chemical Physics Accepted Manuscript

Please do not adjust margins

annealed. Anodization was carried out in a sulfuric acid (H_2SO_4, 20%) solution at room temperature, at the constant current density of 3 A/dm^2. By this procedure, AAO films with pore diameter of 25±5 nm and average interpore spacing of 120±20 nm were obtained. The arrays of silver nanoparticles were formed by a thermal evaporation of silver onto the surface of 60 μm thick AAO template at room temperature. The quoted thickness *h* of the silver film was estimated from the mass of the metal deposited on the area. It was varied by varying the deposition time. Samples with Ag thicknesses of 15, 30, 45, 60, 75, 90, 120, and 150 nm were prepared. The morphology of samples was explored by a Hitachi-S4800 electron microscope with a resolution of 1 nm.

2.2 UV-vis and SERS measurements

UV-vis extinction spectra were recorded on Cary 500 Scan (Varian) spectrophotometer.

Samples for SERS measurements were prepared in two ways. In the first case, Ag/AAO substrates were incubated for 1.5 hours in 3 ml of 10^{-6} M CuTMpyP4 aqueous solution. Samples of the second kind were prepared by deposition a 10 μL drop of 10^{-6} M porphyrin solution onto a surface of Ag/AAO and allowed to air-dry.

SERS spectra were taken using a modular Raman spectrometer based on Spex 270M (Jobin Yvon) spectrograph and liquid-nitrogen cooled CCD detector (Princeton Instruments). Spectra were excited by a 441.6 nm (He-Cd laser) with *s*-polarized incident light at typically 2 ÷ 5 mW power focused on to the sample (laser-spot diameter was ~ 100 μm). A 90° laser beam-to-collecting optics arrangement and a 57° normal of the sample surface-to-laser beam orientation were used.

2.3 Simulations

To identify the resonant plasmonic modes excited in a close-packed Ag NPs layer at the surface of AAO, numerical simulations based on the quasicrystalline approximation (QCA) of the statistical theory of multiple scattering of electromagnetic waves was used.[50] This approach takes into account the coherent multiple-scattering effects in a partially-ordered 2D arrays, i.e. lateral electrodynamic interactions between the particles within an array, as well as the interference between the incident wave and the waves scattered by an array in the forward direction. The lateral electrodynamic interactions between individual particles of an array are considered as interference of multiply scattered waves in a planar close-packed arrangement of scatterers. The optical functions of a single spherical scatterer are specified by the Mie theory. The spatial arrangement of particles within a close-packed 2D array is determined by the radial distribution function calculated in the assumption of hard spheres.[51]

The QCA approach is most effective when the nanoparticle array is close to a crystalline structure. So, we can reasonably apply the QCA to close-packed arrays as they are characterized by short-range ordering: locations of neighbouring particles are partially correlated due to their finite sizes and high concentration. In our simulations we have also taken into account size-dependence of the dielectric function for metallic nanoparticles in the frame of the model of limitation of electron mean free path.[52] The details of the realized calculation scheme can be found in.[53]

In the present paper the extinction spectra of the close-packed 2D arrays of Ag nanospheres have been calculated. The volume fraction of metal *f* was kept constant while the size of nanoparticles was varied for different array samples. Optical constants for bulk silver were taken from the handbook.[54] Dielectric medium with a refractive index of 1.5 (average of refractive indices of AAO and air) was considered as surroundings of NPs. It should be noted that the simulations were carried out disregarding the structural features of the AAO substrate. However, they substantially represent the main trends in spectral appearance of the collective SPR caused by a change in size and/or concentration of NPs in the close-packed array.

3. Results and Discussion

3.1 SEM characterization of Ag/AAO samples

Scanning electron microscopy (SEM) top view and cross-sectional images for Ag/AAO sample with *h* = 60 nm silver mass-thickness are depicted in Fig. 1. As is seen, Ag grain arrays were spontaneously formed at the surface of AAO substrate by thermal deposition. Evidently, regular network of the arrays that create an artificial roughness reflects the regularity of the holes in the AAO template. The dense layer of silver grains with a size of 40-50 nm decorates mainly the necks between the holes, forming a film of about 70 nm thickness, the value corresponding well to that estimated from the mass of Ag deposit. Close contacts between NPs should promote formation of "hot spots" in which strong Raman enhancement for analyte molecules occurs. The almost detached grains with a size of 20-40 nm are randomly distributed over the cap walls as well as on silver layer at the necks. This is consistent with grain growth through coalescence and accretion of deposited silver atoms.[55]

We suggest that the morphology of silver deposition for other samples of various thicknesses is similar. With increasing Ag thickness (e.g. 120 nm) nanoparticles grow and hang slightly over the hole's edges (data not shown). For Ag/AAO samples with thinner silver films thickness (30 and 15 nm) quality of SEM images was not enough satisfactory.

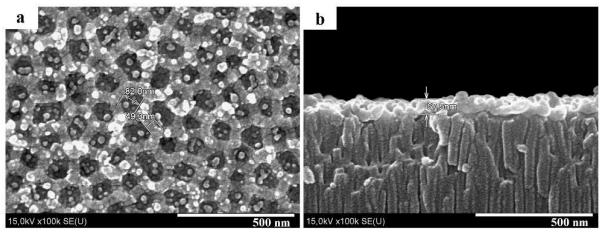

Figure 1. SEM images of Ag/AAO sample with a thickness of silver film ca 60 nm: (a) the top view and (b) the cross-sectional view.

Physical Chemistry Chemical Physics Accepted Manuscript

3.2 UV-vis spectra

Figure 2 shows the effect of silver film mass-thickness *h* on the experimentally measured extinction spectra of Ag/AAO substrates. Extinction spectra were obtained at normal incidence as well as at 57°. The angle of 57° was used because SERS spectra were excited at the same angle (see below). As it is seen from transmission of a bare AAO template without Ag NPs (Fig. 2, dotted curve on 15 nm panel), the AAO prepared in sulfuric acid-based electrolyte is almost transparent throughout the visible region. It shows only gradual absorption increase below 400 nm that should not affect significantly positions of the plasmon resonance maxima. Therefore, it was not necessary to subtract contribution of the bare AAO film from extinction spectra of Ag/AAO samples.

The maxima located at around 400 nm (Fig. 2) can be thus attributed to the SPR of silver nanoarrays formed at the surface of AAO template. The increase of Ag thickness leads to topological transformation of granular layer, e.g. the change in mean size of NPs and their volume concentration in the layer (volume fraction of metal *f*) that results in quantitative as well as qualitative changes of spectral manifestations of the collective SPR of the close-packed NPs array. The general tendency is that the overall extinction increases with the increase of Ag thickness. Furthermore, the SPR maximum varies around 400 nm, the broad band at wavelengths > 550 nm becomes gradually stronger with a concomitant shift of its maximum to infrared. As is evident from Fig. 2, similar spectral behavior can be observed for normal incidence (perpendicular to the substrate surface) as well as for illumination at 57°.

To understand nonmonotonous spectral shift of the maximum of collective SPR band with the increase of Ag mass-thickness *h*, let us first consider LSPR modes of individual metallic nanospheres. In the case of small NPs (with the size less than 10 nm) LSPR modes are dipole in character. Increase in their diameter results in red shift, which is related to the so-called "retardation effect", that is reducing the LSPR frequency due to phase mismatch in oscillations of spatially separated free electrons within the particles of finite size. Another consequence of NPs size increase is emerging of higher-order (quadrupole and then octupole) modes of the LSPR, leading to appearance of several peaks in the spectra. Each arising multipole mode has a non-radiative decay type, yielding absorptive properties of metallic NPs.

With the increase of NP size the contribution from the dipole absorption becomes less important, due to the competition from energy scattering processes, and after exceeding some specific NP size the mode relaxation becomes fully radiative. Thus, size increase changes the decay type of the excited LSPR mode from non-radiative to radiative.[56] In the non-radiative case, all the energy taken out by the metallic NP from the incident light-wave is localized near the nanoparticle surface, forming the regions with significant near-field enhancement ("hot spots"). This regime is the most favorable for SERS amplification. In the case of radiative decay, the energy of the excitation taken out from the incident light is mainly scattered back to the environment.

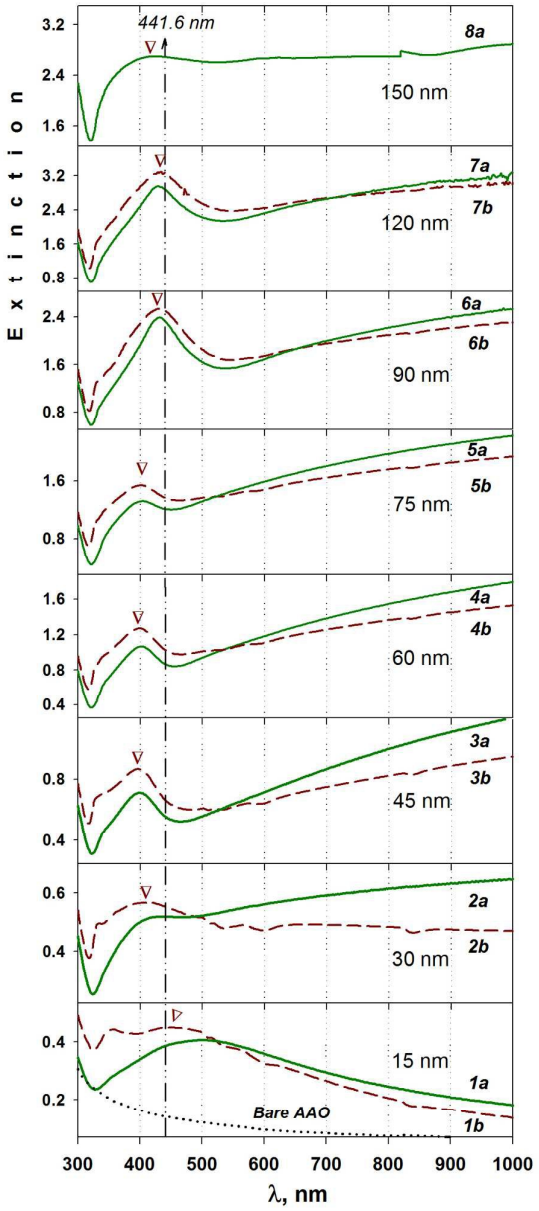

Figure 2. Extinction spectra of Ag/AAO samples with different Ag film thickness: 1a,b - 15 nm; 2 a,b - 30 nm; 3 a,b - 45 nm; 4 a,b - 60 nm; 5 a,b - 75 nm; 6 a,b - 90 nm; 7 a,b - 120 nm; 8a - 150 nm. Spectra 1a – 8a were measured at normal incidence, spectra 1b – 7b at the angle 57°. Dash-dot-dot arrow indicates position of excitation wavelength 441.6 nm.

For a close-packed layer of NPs, the above described mechanisms are significantly more complicated due to the coherent multiple light scattering between neighboring NPs. Such electrodynamical processes lead to collectivization of plasmon excitations: LSPR is transformed into SPR band, accompanied by enlargement of plasmon localization region and a change of SPR spectral manifestation, in particular its frequency shift.[57-59] Moreover, in the narrow gaps between close-packed NPs a manifold strengthening of the local field can occur.[60,61]

Physical Chemistry Chemical Physics Accepted Manuscript

This journal is © The Royal Society of Chemistry 20xx

Please do not adjust margins

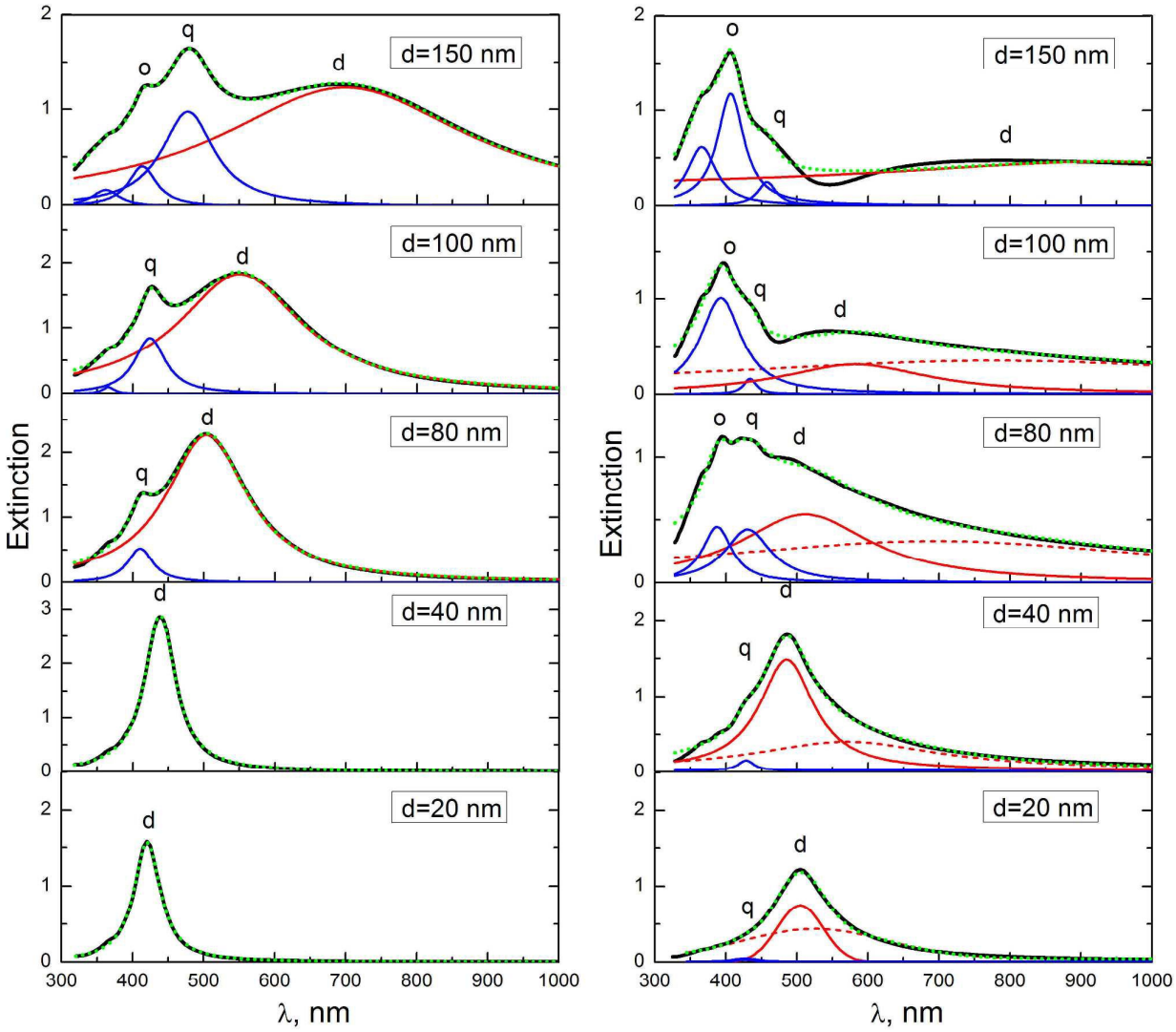

Figure 3. Calculated extinction spectra and tentative assignment of SPR modes for sparse colloids of Ag NPs (left panel) and close-packed monolayers (right panel) of Ag nanospheres of different diameters *d*. d – dipole mode; q – quadrupole mode; o – octupole mode.

In Fig. 3 we show comparison of the calculated extinction spectra for two nanostructure types. The first type corresponds to a close-packed 2D array of silver NPs (Fig. 3. right panel), which models silver nanostructures on the surface of AAO under investigation. Here we consider arrays with different NPs sizes, but identical metal volume fraction, f=0.4. The second type corresponds to sparse layers of the same but non-interacting particles (as NPs in non-aggregated colloids), whose optical properties are completely defined by optical functions of single spheres (Fig. 3. left panel). We compare each close-packed 2D array with sparse NPs of the same particle size to demonstrate the influence of electrodynamic coupling between nanoparticles on the SPR resonances. The calculated extinction spectra are plotted by solid black lines.

To estimate the position and contribution of different plasmon modes in these spectra profiles, we have fitted them with multi-Lorentzian functions. The results of this deconvolution analysis are also shown in Fig. 3. The individual Lorentzian components are depicted by red (for dipole mode) and blue (for higher-order modes) lines, while the sums of all Lorentzians are depicted by dashed green lines (being in very good agreement with calculated black lines).

It can be seen from Fig. 3 (left panel) that for single nanoparticles of small sizes (up to 40 nm) the extinction spectrum is determined by only dipole mode contribution. As the NPs size grows, there appears the contribution of higher order modes (quadrupole, octupole, etc.) in the blue spectral region. The situation for close-packed arrays of NPs is much more complicated. Even for small-sized nanoparticles we can notice contribution of several Lorentzian components. In comparison with the case of single NPs, there appears a contribution from very broad red-shifted band (shown with dashed red lines). We suggest that this band can be attributed to collective delocalized plasmon mode of the whole close-

Physical Chemistry Chemical Physics Accepted Manuscript

packed NPs array. That is the total SPR dipole mode of interacting particles consists from both localized mode of the single particle deposited in the effective field of the other nanoparticles and delocalized mode of the close-packed NPs array.

Moreover, multiple scattering between NPs in a close-packed array leads to intensification of the higher-order SPR modes and to the red shift of all SPR modes. For particles with diameter 20÷40 nm, the close-packed array exhibits (right panel) formation of the quadrupole mode (~430 nm), which is absent in the corresponding extinction spectra of the non-interacting NPs of the same sizes (left panel). For close-packed array made of NPs with diameter 150 nm, there appears a strong extinction band formed by the quadrupole (~ 460 nm) and octupole (~408 nm) SPR modes. Importantly, intensity of the octupole mode greatly exceeds intensity of the quadrupole mode – in contrast to the reverse situation for 150 nm non-interacting NPs. Presumably, this can be due to their excitation by evanescent waves from the neighbouring particles in the dense layer. Similar behaviour has already been simulated[59] for the system of individual metallic nanospheres excited by evanescent plane waves.

Comparing the obtained experimental (Fig. 2) and calculated (Fig. 3, right panel) extinction spectra of the close-packed arrays of Ag NPs, one can see similar trends in the spectral transformation caused by the increase of Ag mass-thickness. Following explanation can be suggested for this observation: initial increase of *h* from 15 to 45 nm is accompanied by increase of NPs sizes, however with approximately constant volume fraction of the metal in the layer. In this case, the delocalized dipole mode exhibits a red shift, while in the blue region there appears a new band due to intensification of higher-order plasmon modes (in the first place a quadrupole mode). Consequently, the extinction band maximum, λ_{max}, exhibits a blue shift with the increase of *h* from 15 to 45 nm.

Further increase of the average size of NPs with the increase of *h* from 45 to 120 nm results in appearance and intensification of the octupole mode in the collective plasmon resonance (for *h*=75 nm and above). In addition, a gradual red shift takes place not only for both, localized and delocalized dipole modes, but also for the quadrupole one. As is evident from Fig. 3, the red shift of high-order modes can be observed for sufficiently large sparse NPs as well as for their close-packed arrays (compare the curves for *d*=150 nm at the left and right panels of Fig. 3, correspondingly). For this reason, in contrast to the mass-thicknesses below 45 nm, the extinction maximum λ_{max} exhibits a red shift for *h* increasing from 45 to 120 nm. Consequently, the dependence of $\lambda_{max}(h)$ has a non-monotonous character.

It should be noted that growth of the average size of NPs in the layer with the increase of Ag thickness can also be attributed to clustering of NPs. This process significantly increases polydispersity of the system, leading to spectral broadening of all (but notably dipole) plasmon resonance modes. However, further increase of the mass of deposited metal results in denser filling of layer's volume by Ag and to smoothening of its structural features. This is the reason why the measured extinction spectrum for *h* =150 nm (Fig. 2) is degraded to such an extent that it loses resonant features for both individual nanoobjects and their agglomerates.

3.3 Dependence of SERS enhancement on silver film thickness

To examine dependence of the SERS intensity on the Ag mass-thickness, SERS spectra of CuTMpyP4 adsorbed on a series of Ag/AAO substrates were measured using the excitation wavelength λ_{ex}=441.6 nm. Spectra were acquired at two excitation geometries, i.e. with a laser beam directed onto the front- and back side of the samples (Fig. 4). SERS spectra of CuTMpyP4 for different Ag mass-thicknesses measured at the front side incidence are shown in Fig. 5. To better illustrate non-monotonous character of the SERS intensity variations with the increase of Ag thickness, intensity of the CuTMpyP4 1365 cm^{-1} band was plotted as function of the silver thickness (Fig. 6). As can be seen, the strongest Raman signal is firstly observed for the Ag layer of 15 nm. Further increase of the silver thickness to 45 - 75 nm is accompanied by a local decrease of the SERS intensity followed by the second intensity maximum for *h*=120 nm. However, the corresponding intensity was only about one third of that for 15 nm.

Thus, two maxima of the SERS enhancement depending on the

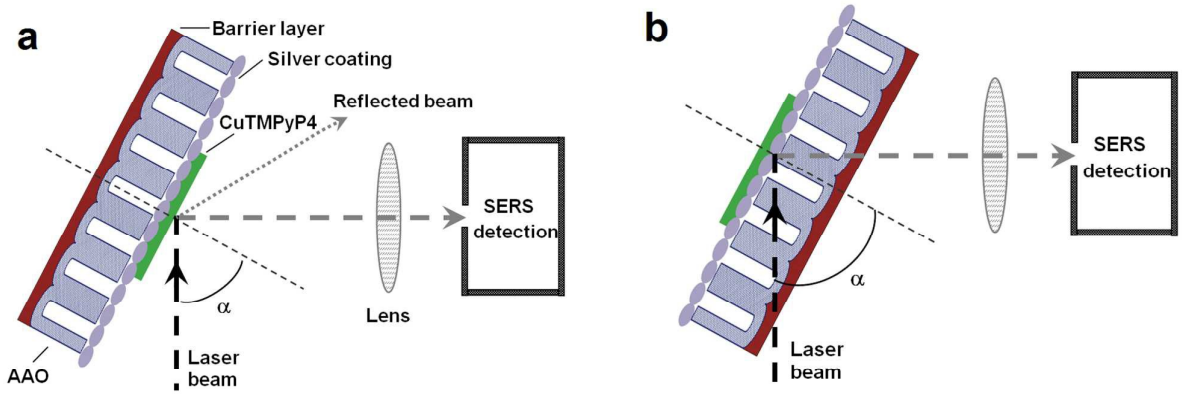

Figure 4. The excitation-detection geometries of SERS measurements: (a) front-side excitation; (b) back-side excitation. Incident angle $\alpha = 57^{o}$.

Physical Chemistry Chemical Physics Accepted Manuscript

This journal is © The Royal Society of Chemistry 20xx

Please do not adjust margins

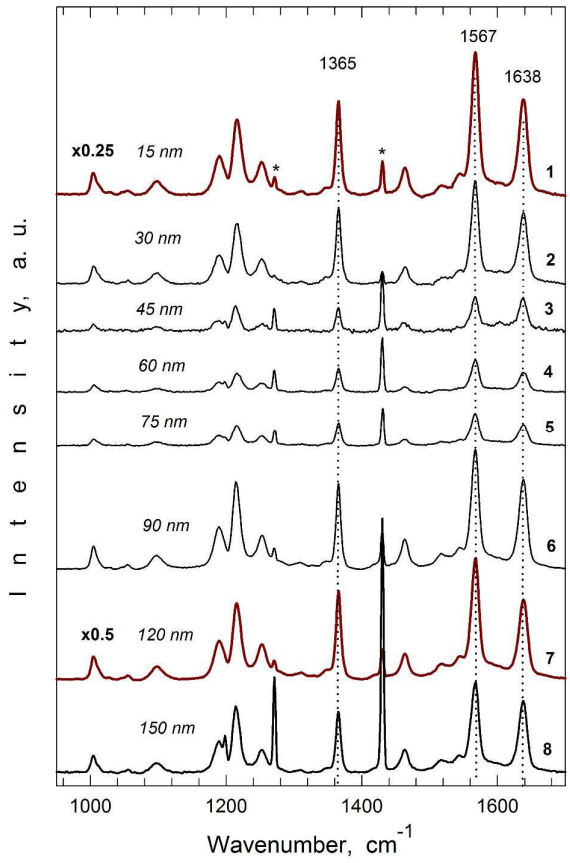

Figure 5. SERS spectra of CuTMpyP4 adsorbed from the 10^{-6} M solution on the surface of Ag/AAO with silver film thickness of 15 (1), 30 (2), 45 (3), 60 (4), 75 (5), 90 (6), 120 (7) and 150 nm (8). Prominent plasma lines of He-Cd laser are marked with asterisks (*).

silver thickness were localized for the excitation 441.6 nm. The same tendency of SERS performance was observed for the second series of samples where analyte molecules were deposited on the silvered surface of AAO by dropping 10 μl of 10^{-6} M porphyrin solution (Fig. 7). Similar results for two series of Ag/AAO samples were obtained for other Raman bands of CuTMpyP4, e.g. 1567 and 1638 cm^{-1} (data not shown).

The non-monotonous dependence of SERS intensity on Ag mass-thickness can be explained taking into account relative positions of the SPR maxima with respect to the excitation wavelength. It must be emphasized that SERS enhancement will be most effective when the excitation is in resonance with respect to the position of a plasmonic mode with non-radiative type of decay, which is damped *via* absorption processes when the energy consumed by NP is localized at the interface.

Dependence of the distance between the extinction maximum and the excitation wavelength (multiplied by a factor of -1) as a function of the Ag mass-thickness is depicted in Fig. 8. Its non-monotonous character with two maxima is close to that observed for SERS intensities (Fig. 6 and 7). It seems that dependence of the SERS activity on the Ag mass-thickness can be attributed mainly to the effectiveness of the overlap between the excitation wavelength and the extinction bands. Upon increase of the thickness of Ag layer, the SPR peak is tuned to overlap with excitation line providing less or more favourable conditions for SERS enhancement. The maximum SERS efficiency is observed for minimal distance between the excitation wavelength and the extinction peak belonging to absorption. In the case of the sample with h=15 nm, the excitation wavelength λ_{ex} falls in the close vicinity of the SPR band attributed to dipole mode. For the samples of greater Ag thickness, the SERS intensity originates mainly from the resonances with pronounced plasmonic modes of higher orders (first quadrupole, then octupole), the relaxations of which have predominantly non-radiative character. It should be emphasized that coincidence of the excitation wavelength and the spectral position of an incipient higher-order plasmon mode with non-radiative damping cannot provide SERS enhancement because of insufficiently strong enhancement of local electromagnetic field near the metallic nanoparticles. Only pronounced resonances can provide an appreciable effect.

As mentioned previously, several studies for free NPs have demonstrated the correlation between LSPR position and SERS intensity depending on the NPs shape and excitation

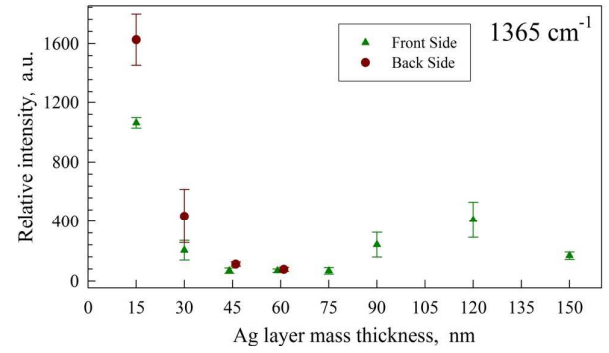

Figure 6. Intensity of the 1365 cm^{-1} band in SERS spectra of CuTMpyP4 adsorbed on the silvered surface of AAO as a function of the silver film thickness. Data obtained at front- and back-side geometry of excitation are depicted by triangles and circles, respectively. The symbols for samples of h=45 nm and h=60 nm have been horizontally offset for clarity.

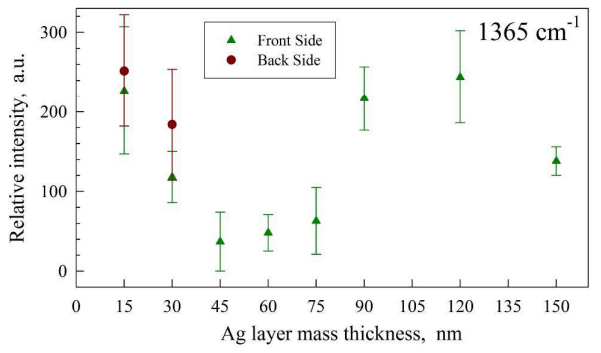

Figure 7. Intensity of the 1365 cm^{-1} band in SERS spectra of CuTMpyP4 deposited on the silvered surface of AAO by dropping from 10 μl of 10^{-6} M solution as a function of the silver film thickness. Data obtained at front- and back-side geometry of excitation are depicted by triangles and circles, respectively.

Physical Chemistry Chemical Physics Accepted Manuscript

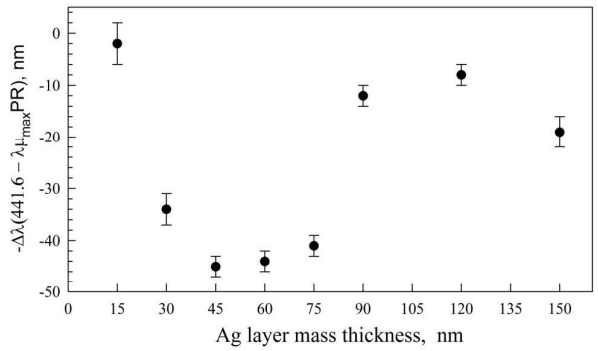

Figure 8. Difference between position of extinction maximum and excitation wavelength as a function of the silver film thickness. Peak maxima were determined for spectra measured at incident angle $\alpha = 57^{o}$.

wavelength.[22-27,31] The influence of multipole modes of LSPR on SERS signal intensity was also investigated. It has been shown for the elongated nanoparticles that the high-orders LSPR modes provide a contribution to the SERS signal.[25,63,64] In the case of metallic nanowires the enhancement obtained for multipole LSPR appeared larger than that achieved for dipolar modes.[25] However, for the arrays of coupled nanoparticles the effect of multipole modes on the SERS performance was insufficiently explored. Especially an issue concerning the role of SPR relaxation in SERS enhancement, i.e. whether it is intrinsic damping within the NPs or radiative damping, was not considered.

Our results indicate that for the nanostructures of tightly coupled Ag NPs such as Ag/AAO the SERS enhancement is strongly dependent on the matching of laser line to non-radiative SPR modes. Moreover we demonstrate the importance of the higher order SPR modes, which are mainly of non-radiative character, in governing the SERS intensity at a given excitation wavelength. It should be emphasized, that the observed SPR–SERS dependence is qualitative. Since the SPR bands are rather broad, it is difficult to assign SPR peak to a particular high order mode. It is possible that extinction maxima used to evaluate closeness to excitation wavelength depicted in Fig. 8 are in reality overlaps of two or more multiple SPR bands.

3.4 Increase of SERS signal at back-side geometry of the excitation

SERS enhancement was investigated for two excitation geometries, the front-side and the back-side (Fig. 4A and 4B, respectively). To average possible inhomogeneities of Ag surface, several spectra were collected for each sample from different spots inside a restricted area (~ 8 mm^2). The SERS intensities of the 1365 cm^{-1} band of CuTMPyP4 deposited on silver film surface *via* soaking of Ag/AAO samples in the analyte solution and by drop-coating are plotted in Fig. 6 and 7 as a function of Ag mass-thickness, respectively. However, with the back-side excitation we have succeeded to record only the spectra for Ag mass-thickness less than 60 nm. In the case of drop coated samples we were not able to obtain spectrum even for 45 nm silver film because of extremely weak Raman signal. It seems that at the back-side geometry, the thick layer of Ag impedes the excitation radiation to reach the analyte molecules. For both sample series and Ag mass-thickness h=15 – 60 nm, the SERS intensities for the back-side excitation were consistently higher than obtained for front-side geometry. The ratio between the average peak intensities for Ag thickness increasing from 15 to 60 nm at two excitations geometries was 1.12, 1.55 and 1.42, 2.18, 1.57, 1.15 for droplet and soaked samples, respectively.

The higher SERS signal for the excitation through dielectric medium than for the excitation through air has been reported earlier in several papers.[65-68] However, the origin of this additional enhancement was not satisfactorily explained for a long time. In the work[65] the additional SERS enhancement for silver/indium island films on glass slides was suggested to be due to 'first layer effect', when the analyte molecules closest to the enhancing field generate the highest signal. This suggestion was later disproved, because the extra enhancement was also observed for a monolayer of analyte molecules.[66] Recently extra SERS signal for silver film on glass at the back-side excitation geometry has been detected.[67] By analysis of Fresnel reflection and transmission terms, a simple physical explanation of this phenomenon was suggested based on the phase shift of light at the dielectric-air interface. The improved intensity of the SERS spectrum from gold and silver particles was observed, when the light was transmitted through the quartz slide instead of direct illumination of molecules.[68] The theoretical model was used to show the impact of the dielectric environment on the enhancement, i.e. the light transmitted through the quartz substrate seems to excite more effectively the localized surface plasmons than the light passing through air and the analytes.

The silver coated AAO substrates used in the present work considerably differ from those investigated previously in,[67,68] as concerns morphology of Ag deposits as well as geometry of underlying AAO template and its refractive index. It should be noted that our observations neither confirm nor disclaim the explanation of the discussed phenomenon proposed in above mentioned studies, and further work on different SERS-active materials is required to fully explore this effect. Nevertheless, the extra enhancement of the SERS intensity due to appropriate excitation geometry described here can be useful for design of more sensitive SERS-based sensors.

Conclusions

A series of silvered AAO samples was prepared and investigated with the aim to clarify effect of mass-thickness of granular Ag layer on the SPR position as well as SERS efficiency. To characterize the SERS responses from Ag/AAO substrates, water-soluble cationic porphyrin CuTMPyP4 was used as a SERS-reporting molecule. Analyzing dependencies of the 1365, 1567, and 1638 cm^{-1} band intensities as function of the Ag mass-thickness, two maxima of SERS enhancement for 441.6 nm excitation were detected for Ag layers of 15 nm and 120 nm. This dependency was ascribed to the effect of the proximity of the excitation wavelength to the maximum of the SPR band of Ag/AAO substrate.

Physical Chemistry Chemical Physics Accepted Manuscript

 This journal is © The Royal Society of Chemistry 20xx

Please do not adjust margins

An important role of the decay type and order of the SPR modes in SERS enhancement efficiency was suggested based on QCA numerical simulations. The layer of close-packed Ag NPs of the size greater than 50 nm exhibits not only dipole but also higher order SPR modes (qudrupole, octupole, etc.) contributing to rather complicated extinction spectra. The most effective SERS excitation wavelengths are those which coincide with the position of the pronounced SPR mode having essentially non-radiative decay. We also demonstrate that spectral position of the collective SPR with non-radiative decay can be effectively tuned by variation of size and concentration of nanoparticles in silver layer.

Consequently, to design the arrays of coupled NPs with maximal SERS enhancement one should take into account not only optimal structural parameters of the substrates but also position of the non-radiative multiple plasmon modes with respect to the excitation wavelength. Moreover additional increase of SERS intensity for the thin metal films can be achieved by use of back-side geometry of excitation. These findings pave the way to more sensitive analytical applications of SERS.

Acknowledgements

This work was supported by the State Scientific Program of Belarus "Electronics and Photonics 2.3.06" and the Czech Science Foundation (P208/10/0941).

References

1 K. Kneipp, H. Kneipp, I. Itzkan, R.R. Dasari and M.S. Feld, *Chem. Rev.*, 1999, **99**, 2957-2975.
2 K. Kim and K.S. Shin, *Anal. Sci*., 2011, **27**, 775-783.
3 S. Cîntă Pînzaru, I. Pavel, N. Leopold and W. Kiefer, *J. Raman Spectrosc.*, 2004, **35**, 338-346.
4 J.M. Reyes-Goddard, H. Barr and N. Stone, *Photodiagn. Photodyn. Ther.*, 2005, **2**, 223-233.
5 J. Kneipp, H. Kneipp and K. Kneipp, *Chem. Soc. Rev.*, 2008, **37**, 1052-1060.
6 K.W. Kho, C.Y. Fu, U.S. Dinish and M. Olivo, *J. Biophotonics*, 2011, **4**, 667-684.
7 Y.C. Tsai, P.C. Hsu, Y.W. Lin and T.M. Wu, *Sens. Actuators B*, 2009, **138**, 5-8.
8 P.R. Stoddart and D.J. White, *Sens. Actuators B*, 2009, **138**, 5-8.
9 S. Boyd, M.F. Bertino, D. Ye, L.S. White and S.J. Seashols, *J. Forensic Sci.*, 2013, **58**, 753-756.
10 Y. Yang, Z.Y. Li, K. Yamaguchi, M. Tanemura, Z.R. Huang, D.L. Jiang, Y.H. Chen, F. Zhou and M. Nogami, *Nanoscale*, 2012, **4**, 2663-2669.
11 R. Halvorson and P.J. Vikesland, *Environ. Sci. Technol.*, 2010, **44**, 7749-7755.
12 R. Aroca, *Surface-Enhanced Vibrational Spectroscopy*, J. Wiley, Chichester, 2006.
13 R.J.C. Brown and M.J.T. Milton, *J. Raman Spectrosc.*, 2008, **39**, 1313-1326.
14 M. Moskovits, *Rev. Mod. Phys*., 1985, **57**, 783-826.
15 H. Xu, J. Aizpurua, M. Kal and P. Apell, *Phys. Rev. E*, 2000, **62**, 4318-4324.
16 G. Vidal and J.B. Pendry, *Phys. Rev. Lett.*, 1996, **77**, 1163
17 J.R. Lombardi, R.L. Brike, T. Lu and J. Xu, *J. Chem. Phys.*, 1986, **84**, 4174.
18 A. Otto, I. Mrozek, H. Grabhorn and W. Akemann, *J. Phys.: Condens. Matter.*, 1992, **4**, 1143-1212.
19 S.J. Lee, A.R. Morrill and M.J. Moscovits, *J. Am. Chem. Soc.*, 2006, **128**, 2200-2201.
20 A.J. Haes and R.P. Van Duyne, *J. Am. Chem. Soc.*, 2002, **124**, 10596.
21 K. Kneipp, Y. Wang, H. Kneipp, L.T. Perelman, I. Itzkan, R.R. Dasari and M.S. Feld, *Phys. Rev. Lett.*, 1996, **78**, 1667.
22 C.L. Haynes and R.P. Van Duyne, *J. Phys. Chem. B*, 2003, **107**, 7426–7433.
23 N. Félidj, J. Aubard, G. Levi, J.R. Krenn, A. Hohenau, G. Schider, A. Leitner and F.R. Aussenegg, Appl. Phys. Lett. 2003. 82, 3095–3097.
24 J. Grand, M. Lamy de la Chapelle, J.L. Bijeon, P.M. Adam, A. Vial and P. Royer, *Phys. Rev*., 2005, **72**, 33407.
25 L. Billot, M. Lamy de la Chapelle, A.-S. Grimault, A. Vial, D. Barchiesi, J.-L. Bijeon, P.-M. Adam and P. Royer, *Chem. Phys. Lett*., 2006, **422**, 303–307.
26 N. Guillot and M. Lamy de la Chapelle, *J. Quant. Spectrosc. Radiat. Transfer*., 2012, **113**, 2321-2333.
27 N. Guillot, H. Shen, B. Frémaux, O. Péron, E. Rinnert, T. Toury and M. Lamy de la Chapelle, *Appl. Phys. Lett*., 2010, **97**, 023113.
28 M.K. Hossain, G.R. Willmott, P.G. Etchegoin, R.J. Blaikie and J.L. Tallon, *Nanoscale*, 2013, **5**, 8945-8950.
29 A. Lamberti, A. Virga, A. Angelini, A. Ricci, E. Descrovi, M. Cocuzza and F. Giorgis, *RSC Adv.*, 2015, **5**, 4404-4410.
30 M. Kang, J.-J. Kim, Y.-J. Oh, S.-G. Park and K.-H. Jeong, *Adv. Mater.*, 2014, **26**, 4510-4514.
31 A.D. McFarland, M.A. Young, J.A. Dieringer and R.P. Van Duyne, *J. Phys. Chem. B*, 2005, **109**, 11279-11285.
32 L. Gunnarsson, E.J. Bjerneld, H. Xu, S. Petronis, B. Kasemo and M. Kall, *Appl. Phys. Lett*., 2001, **78**, 802-804.
33 Y.-J. Liu, Z.-Y. Zhang, Q. Zhao and Y.-P. Zhao, *Appl. Phys. Lett*., 2008, **93**, 173106–173123.
34 T. Tan, C. Tian, Z. Ren, J. Yang, Y. Chen, L. Sun, Z. Li, A. Wu, J. Yin and H. Fu, *Phys. Chem. Chem. Phys*., 2013, **15**, 21034-21042.
35 L. Wang, Y. Sun and Z. Li, *Appl. Surf. Sci*., 2015, **325**, 242-250.
36 B.L. Broglin, A. Andreu, N. Dhussa, J.A. Jr. Heath, J. Gerst, B. Dudley, D. Holland and M. El-Kouedi, *Langmuir*, 2007, **23**, 4563-4568.
37 K.G. Biswas, H. El Matbouly, V. Rawat, J.L. Schroeder and T.D. Sands, *Appl. Phys. Lett*., 2009, **95**, 073108.
38 V.G. Stoleru and E. Towe, *Microelectron. Eng*., 2005, **81**, 358-365.
39 Z. Lu, W. Ruan, J. Yang, W. Xu, C. Zhao and B. Zhao, *J. Raman Spectrosc.*, 2009, **40**, 112-116.
40 H. Ko and V.V. Tsukruk, *Small*, 2008, **4**, 1980-1984.
41 N. Ji, W. Ruan, C. Wang, Z. Lu and B. Zhao, *Langmuir*, 2009, **25**, 11869-11873.
42 J. Wang, L. Huang, L. Yuan, L. Zhao, X. Feng, W. Zhang, L. Zhai and J. Zhu, *Appl. Surf. Sci.*, 2012, **258**, 3519-3523.
43 N. Ji, W. Ruan, Z. Li, C. Wang, Z. Yang and B. Zhao, *J. Raman Spectrosc.*, 2013, **44**, 1-5.
44 K. Malek, A. Brzózka, A. Rygula and G.D. Sulka, *J. Raman Spectr.*, 2014, **45**, 281-291.
45 T. Kondo, H. Miyazaki, K. Nishio and H. Masuda, *J. Photochem. Photobiol. A*, 2011, **221**, 199-203.
46 J. Lin, H. Lan, W. Zheng, Y. Qu and F. Lai, *NANO*, 2012, **7**, 1250048.
47 S.N. Terekhov, P. Mojzes, S.M. Kachan, N.I. Mukhurov, S.P. Zhvavyi, A.Yu. Panarin, I.A. Khodasevich, V.A. Orlovich, A. Thorel, F. Grillon and P.-Y. Turpin, *J. Raman Spectrosc.*, 2011, **42**, 12-20.
48 R.F. Pasternack, E.J. Gibbs and J.J. Vilafranca, *Biochemistry*, 1983, **22**, 2406-2414.

Physical Chemistry Chemical Physics Accepted Manuscript

49 H. Masuda and M. Satoh, *Jpn. J. Appl. Phys.*, 1996, **35**, L126-L129.
50 K.M. Hong, *J. Opt. Soc. Am.*, 1980, **70**, 821-826.
51 J. Ziman, *Models of Disorder*, Cambridge University Press, Cambridge, 1979.
52 U. Kreibig and C.V. Fragstein, *Zeitschrift für Physik*, 1969, **224**, 307-323.
53 S.M. Kachan and A.N. Ponyavina, *J. Phys.: Condens. Matter.*, 2002, **14**, 103-111.
54 *Handbook of Optical Constants of Solids*, ed. E.D. Palik, Academic Press, New York, 1991.
55 N. Pavenayotin,; M.D. Jr. Stewart, J.M. Jr.Valles, A. Yin and J.M. Xu, *Appl. Phys. Lett.*, 2005, **87**, 193111.
56 K. Kolwas and A. Derkachova, *J. Quant. Spectrosc. Radiat. Transfer.*, 2013, **114**, 45-55.
57 L. Gunnarsson, T. Rindzevicius, J. Prikulis, B. Kasemo, M. Käll, S. Zou and G.C. Schatz, *J. Phys. Chem. B*, 2004, **109**, 1079-1087.
58 W. Rechberger, A. Hohenau, A. Leitner, J.R. Krenn, B. Lamprecht and F.R. Aussenegg *Opt. Commun.*, 2003, **220**, 137-141.
59 A. Farhang and O. Martin, *Opt. Express.*, 2011, **19**, 11387-11396.
60 P.K. Jain, and M.A. El-Sayed, *Chem. Phys. Lett.*, 2010, **487**, 153-164.
61 N.J. Halas, S. Lal, W.-S. Chang, S. Link and P. Nordlander, *Chem. Rev.*, 2011, **111**, 3913-3961.
62 M. Quinten, A. Pack and R. Wannemacher, *Appl. Phys. B: Lasers Opt.*, 1999, **68**, 87-92.
63 G. Laurent, N. Félidj, J. Aubard, G. Lévi, J. R. Krenn, A. Hohenau, G. Schider, A. Leitner, and F. R. Aussenegg, *Phys. Rev. B*, 2005, **71**, 045430.
64 G. Laurent, N. Félidj, J. Aubard, G. Levi, J.R. Krenn, A. Hohenau, G. Schider, A. Leitner and F. R. Aussenegg, *J. Chem. Phys.*, 2005, **122**, 011102-011104.
65 C. Jennings, R. Aroca, A. M. Hor and R.O. Loutfy, *Anal. Chem.*, 1984, **56**, 2033-2035.
66 R. Aroca, C. Jennings, G.K. Kovacs, R.O. Loutfy and P.S. Vincett, *J. Phys. Chem.,* 1985, **89**, 4051-4054.
67 S. Jayawardhana, L. Rosa, S. Juodkazis and P.R. Stoddart, *Sci. Rep.*, 2013, **3**, 2335.
68 S. Funke and H. Wackerbarth, *J. Raman Spectr.*, 2013, **44**, 1010-1013.

Physical Chemistry Chemical Physics Accepted Manuscript

This journal is © The Royal Society of Chemistry 20xx

Please do not adjust margins